Oxide confinement and high contrast grating mirrors for Mid-infrared VCSELs

Youness Laaroussi, Christyves Chevallier, Frédéric Genty, Nicolas Fressengeas, Laurent Cerutti, Thierry Taliercio, Olivier Gauthier-Lafaye, Pierre-François Calmon, Benjamin Reig, Joël Jacquet, et al.

Oxide confinement and high contrast grating mirrors for Mid-infrared VCSELs

Youness Laaroussi,[1,2] Christyves Chevallier,[3] Frédéric Genty,[3] Nicolas Fressengeas,[3] Laurent Cerutti,[2] Thierry Taliercio,[2] Olivier Gauthier-Lafaye,[1] Pierre-François Calmon,[1] Benjamin Reig,[1] Joel Jacquet,[3] and Guilhem Almuneau[1,*]

[1]CNRS ; LAAS ; 7 avenue du colonel Roche, F-31077 Toulouse Cedex 4, France Université de Toulouse ; UPS, INSA, INP, ISAE ; UT1, UTM, LAAS ; F-31077 Toulouse Cedex 4, France

[2]Université Montpellier 2; Institut d'Electronique du Sud; UMR 5214 CNRS; Place Eugène Bataillon, F-34095 Montpellier Cedex 5, France

[3]LMOPS, EA n°4423 Université de Lorraine et Supélec, 2 rue Edouard Belin, 57070 Metz, France

[*]almuneau@laas.fr

Abstract: A new mid-infrared (MIR) Vertical Cavity Surface Emitting Laser (VCSEL) structure is proposed. We have integrated to the VCSEL structure both an oxide aperture for lateral confinement, and a sub-wavelength high-contrast-grating top mirror. Upon the GaSb-based half-VCSEL, we have grown a metamorphic AlGaAs heterostructure to enable thermal oxidation and grating mirror fabrication steps. A methodology based on optimization and anti-optimization methods has been used to design the optical grating, with improved parameter tolerances regarding processing errors. Finally, we show the complete fabrication of an electrically-pumped MIR monolithic VCSEL structure implementing both oxide confinement and a subwavelength grating top mirror.

OCIS codes: (140.3070) Infrared and far-infrared lasers; (140.7260) Vertical cavity surface emitting lasers; (050.6624) Subwavelength structures; (220.0220) Optical design and fabrication.

References and links

1. S. Arafin, A. Bachmann, K. Kashani-Shirazi, and M.-C. Amann, "Electrically pumped continuous-wave vertical-cavity surface-emitting lasers at ~2.6 µm," Appl. Phys. Lett. **95**(13), 131120 (2009).
2. A. Ducanchez, L. Cerutti, P. Grech, F. Genty, and E. Tournié, "Mid-infrared GaSb-based EP-VCSEL emitting at 2.63 µm," Electron. Lett. **45**(5), 265–266 (2009).
3. R. Hanfoug, A. Salesse, D. A. Yarekha, A. N. Baranov, and C. Alibert, "Use of AlOx in cladding layers of an antimonide laser structure emitting at 2.3 µm," Semicond. Sci. Technol. **16**(11), 936–938 (2001).
4. Y. Laaroussi, *et al*., "Oxide-confined mid-infrared VCSELs," Electron. Lett. **48**(25), 1616–1618 (2012).
5. J. Kennedy and R. Eberhart, "Particle swarm optimization," in *Proceedings of IEEE International Conference on Neural Networks* (IEEE 1995) **4**, pp. 1942–1948.
6. I. Elishakoff, R. Haftka, and J. Fang, "Structural design under bounded uncertainty– Optimization with anti-optimization," Comput. Struc. **53**(6), 1401–1405 (1994).
7. P. Lalanne, J. P. Hugonin, and P. Chavel, "Optical properties of deep lamellar gratings: A coupled bloch-mode insight," J. Lightwave Technol. **24**(6), 2442–2449 (2006).
8. V. Karagodsky, F. G. Sedgwick, and C. J. Chang-Hasnain, "Theoretical analysis of subwavelength high contrast grating reflectors," Opt. Express **18**(16), 16973–16988 (2010).
9. S. Goeman, S. Boons, B. Dhoedt, K. Vandeputte, K. Caekebeke, P. Van Daele, and R. Baets, "First demonstration of highly reflective and highly polarization selective diffraction gratings (GIRO-gratings) for long-wavelength VCSELs," IEEE Photon. Technol. Lett. **10**(9), 1205–1207 (1998).
10. C. Mateus, M. Huang, L. Chen, C. Chang-Hasnain, and Y. Suzuki, "Broad-band mirror (1.12-1.62 µm) using a subwavelength grating," IEEE Photon. Technol. Lett. **16**(7), 1676–1678 (2004).
11. L. Cerutti, A. Ducanchez, G. Narcy, P. Grech, G. Boissier, A. Garnache, E. Tournié, and F. Genty, "GaSb-based VCSELs emitting in the mid-infrared wavelength range (2-3 µm) grown by MBE," J. Cryst. Growth **311**(7), 1912–1916 (2009).
12. S. Boutami, B. Benbakir, J.-L. Leclercq, and P. Viktorovitch, "Compact and polarization controlled 1.55 µm vertical-cavity surface-emitting laser using single-layer photonic crystal mirror," Appl. Phys. Lett. **91**(7), 071105 (2007).
13. M. C. Huang, Y. Zhou, and C. J. Chang-Hasnain, "Polarization mode control in high contrast subwavelength grating VCSEL," in *Conference on Lasers and Electro-Optics/Quantum Electronics and Laser Science*

#192341 - $15.00 USD Received 18 Jun 2013; revised 8 Aug 2013; accepted 8 Aug 2013; published 3 Sep 2013

Conference and Photonic Applications Systems Technologies (Optical Society of America, 2008), paper CMGG5.
14. H. Sano, J. Kashino, A. Gerke, A. Imamura, F. Koyama, and C. J. Chang-Hasnain, "Transverse mode control of VCSELS with high contrast sub-wavelength grating functioning as angular filter," in *CLEO: Science and Innovations* (Optical Society of America 2012), paper CW3N.5.
15. G. Almuneau, M. Condé, O. Gauthier-Lafaye, V. Bardinal, and C. Fontaine, "High reflectivity monolithic sub-wavelength diffraction grating with GaAs/AlOx stack," J. Opt. **13**(1), 015505 (2011).
16. M. G. Moharam, D. A. Pommet, E. B. Grann, and T. K. Gaylord, "Stable implementation of the rigorous coupled-wave analysis for surface-relief gratings: enhanced transmittance matrix approach," J. Opt. Soc. Am. A **12**(5), 1077–1086 (1995).
17. C. Chevallier, N. Fressengeas, F. Genty, and J. Jacquet, "Optimized sub-wavelength grating mirror design for mid-infrared wavelength range," Appl. Phys. A-Mater. **103**(4), 1139–1144 (2011).
18. H. Wu, W. Mo, J. Hou, D. Gao, R. Hao, H. Jiang, R. Guo, W. Wu and Zhou, "A high performance polarization independent reflector based on a multilayered configuration grating structure," J. Opt. **12**, 065703 (2010).
19. Y. Zhou, M. Huang, and C. Chang-Hasnain, "Large fabrication tolerance for VCSELs using high-contrast grating," IEEE Photon. Technol. Lett. **20**(6), 434–436 (2008).
20. C. Chevallier, N. Fressengeas, F. Genty, and J. Jacquet, "Robust design of Si/Si_3N_4 high contrast grating mirror for mid-infrared vcsel application," Opt. Quantum Electron. **44**(3-5), 169–174 (2012).
21. C. Chevallier, N. Fressengeas, F. Genty, and J. Jacquet, "Mid-infrared sub-wavelength grating mirror design: tolerance and influence of technological constraints," J. Opt. **13**(12), 125502 (2011).
22. S. Huang, G. Balakrishnan, and D. Huffaker, "Interfacial misfit array formation for GaSb growth on GaAs," J. Appl. Phys. **105**(10), 103104 (2009).
23. J. B. Rodriguez, L. Cerutti, and E. Tournié, "GaSb-based, 2.2 μm type-I laser fabricated on GaAs substrate operating continuous wave at room temperature," Appl. Phys. Lett. **94**(2), 023506 (2009).
24. J. R. Reboul, L. Cerutti, J. B. Rodriguez, P. Grech, and E. Tournié, "Continuous)wave operation above room temperature of GaSb-based lasers diodes grown on Si," Appl. Phys. Lett. **99**(12), 121113 (2011).
25. S. H. Huang, G. Balakrishnan, M. Metha, A. Koshakhlagh, L. R. Dawson, and D. L. Huffaker, "Epitaxial growth and formation of interfacial misfit array for tensile GaAs on GaSb," Appl. Phys. Lett. **90**(16), 161902 (2007).
26. C. Raisin, A. Rocher, G. Landa, R. Carles, and L. Lassabatère, "GaSb/GaAs heteroepitaxy characterized as a stress-free system," Appl. Surf. Sci. **50**(1-4), 434–439 (1991).
27. G. Almuneau, *et al*., "Real-time in situ monitoring of wet thermal oxidation for precise confinement in VCSELs," Sep. Sci. Technol. **23**, 105021 (2008).
28. Y. Laaroussi, G. Almuneau, D. Sanchez, and L. Cerutti, "Efficient lateral confinement by an oxide aperture in a mid-infrared GaSb-based vertical light-emitting source," J. Phys. D **44**(14), 142001 (2011).
29. R. Hanfoug, A. Salesse, D. A. Yarekha, A. N. Baranov, and C. Alibert, "Use of AlOx in cladding layers of an antimonide laser structure emitting at 2.3 μm," Semicond. Sci. Technol. **16**(11), 936–938 (2001).

1. Introduction

Vertical-cavity surface-emitting lasers (VCSEL) have already demonstrated their excellent ability as compact sources for molecular spectroscopic measurements. For these applications, the mid-infrared (MIR) wavelengths ($\lambda > 2$ μm) represents a major field of investigations since they allow the detection of molecules in various domains including environment (polluting gas detection,...), medicine (illness diagnostics, ...), food market or industrial process control (gas emission during process, security, ...). A general issue for the long-wavelength VCSELs is the inherent thick epitaxial structure (about $t = 14\mu m$ for $\lambda = 2.3$ μm) leading to detrimental electro-thermo-optical properties. Although, for emission at $\lambda > 2$ μm, the antimonide alloys are the better system to reach high performance lasers, this system still suffer from the lower development of the material processing technology compared to the conventional GaAs and InP options. Nevertheless, excellent results have been recently demonstrated near 2.3 μm and 2.6 μm with monolithic, or hybrid dielectric-semiconductor Sb-based structures [1,2]. Moreover, even if InP-based technology allows high performing electrically-pumped (EP) VCSELs up to 2.3 μm, emission beyond 2.6 μm can only be realized with GaSb-based active layers. In this paper, we propose to integrate both a lateral oxide electrical / optical confinement, and a sub-wavelength grating high contrast mirror (HCG), within a Sb-based VCSEL structure emitting in the MIR spectral range. In order to define a simple and proven way for electro-optical confinement, we propose to use a metamorphic approach with (Al)GaAs layer to be oxidized [3,4]. This approach combines the advantages of a well-controlled oxidation of an AlGaAs layer with the high-efficiency of a Sb-based active region for emission in the MIR. In addition, in order to overcome the problems caused by the laser structure thickness and the inherent electro-optical-thermal issues, the use of HCG mirror allows to control directly through its design the lasing

#192341 - $15.00 USD Received 18 Jun 2013; revised 8 Aug 2013; accepted 8 Aug 2013; published 3 Sep 2013

wavelength, to stabilize the beam polarization while maintaining transverse single-mode operation. In this work, since its optical properties depend on multiple geometrical parameters, the HCG design is refined by an original method of optimization based on particle swarm optimization algorithm [5] combined with an anti-optimization one [6]. Moreover, the development of this mirror implies technological targets as the etching control of semiconductor alloys on a nanometric scale, but also the wet oxidation of these alloys. We finally present the results obtained on electrically-pumped characterizations of MIR-VCSELs structures, for which we included an oxide aperture for lateral confinement and a HCG as the top high-reflectivity output mirror, both based on Al_xO_y/GaAs heterostructures.

2. Optimization Method for the design of MIR HCG-VCSELs

2.1 High contrast grating mirror structure

A HCG is composed of a diffraction grating with a high index contrast between the slab and surrounding materials. By tailoring the period of the grating to sub-wavelength dimensions, one suppresses all the diffraction orders, except the 0th order. In such a regime, it has been shown that [7, 8] very high reflectivity on a wide spectral band can be achieved when the two or more propagating Bloch modes sustained by the grating waveguide interfere destructively at the output interface, thus cancelling each other in the transmission through the grating, and reflecting back all the incident power.

Therefore, a properly-designed HCG mirror is an extremely efficient mirror with almost 100% reflectivity over a large bandwidth which can reach $\Delta\lambda/\lambda_0$ = 30% [9,10]. This extraordinary optical property makes HCG very attractive to replace Bragg reflectors in VCSELs by using only one layer, instead of about twenty or more quarter wavelength layers required in the case of MIR VCSELs [11]. Furthermore, besides a 10 fold reduction in thickness, HCG mirrors are polarization sensitive due to their 1D symmetry and can be designed to fix the polarization of VCSEL structures [9,12,13].

Another asset of the HCG structures is that one can take advantage of the highly angular dependent reflectivity to ensure that laser emission can only be obtained on the fundamental transverse mode [14].

The HCG structure presented in Fig. 1 is made of a GaAs grating (n = 3.3) with a period Λ, a groove width L_e, a slab width L_f and a thickness T_g. The grating layer is combined to an Al_xO_y low index layer (n = 1.66) of thickness T_A obtained by wet oxidation of an $Al_{0.98}GaAs$ layer [15]. The GaAs grating layer is not completely etched resulting in a GaAs sublayer of thickness T_L to prevent delamination during the oxidation process and enhance mirror performances.

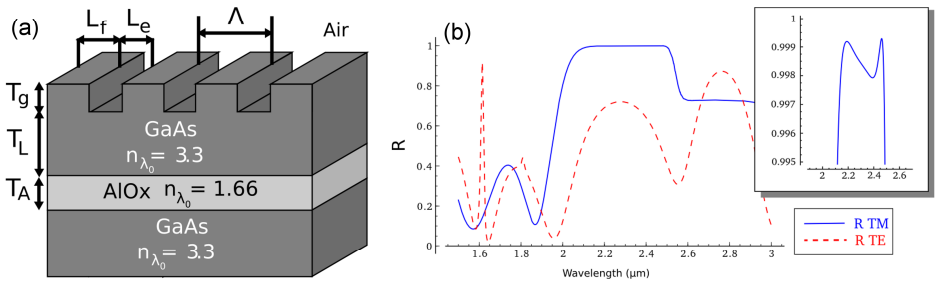

Fig. 1. Design of the HCG mirror structure. (a) Scheme of the GaAs/Al_xO_y high contrast grating structure. The light propagates upwards from the GaAs substrate at normal incidence. (b) Reflectivity spectra for transverse magnetic (TM) and transverse electric (TE) modes of the optimum design exhibiting a 369 nm large and 99.5% high reflectivity stopband for R_{TM}. A good polarization selectivity is obtained with R_{TE}<80% for the whole stopband.

#192341 - $15.00 USD Received 18 Jun 2013; revised 8 Aug 2013; accepted 8 Aug 2013; published 3 Sep 2013

2.2 Design method

The reflectivity of the grating structure is numerically computed for transverse magnetic (TM) and transverse electric (TE) modes by rigorous coupled-wave analysis (RCWA) [16]. The light excitation is at normal incidence to the grating surface and propagates from the substrate as it is the case in the studied VCSEL configuration. To ensure laser emission with improved polarization stability, the HCG is designed to provide a reflectivity R_{TM}>99.5% while keeping R_{TE} below 90% for the largest possible bandwidth (cf. Figure 1(b)). These requirements are quantitatively defined by a merit factor *MF* which mainly represents the normalized bandwidth $\Delta\lambda/\lambda_0$ centered at λ_0 multiplied by a Gaussian weighted average of the reflection coefficient R_{TM} [17].

The parameters of the design are then automatically adjusted by a particle swarm optimization algorithm (PSOA) [5] which maximizes *MF*, and thus provides the best HCG mirror for the VCSEL application.

From a technological point a view, it is important to have not only a design that exhibits good performances, but also large fabrication tolerances. HCGs have been shown to exhibit good tolerance values of more than 20 nm on the different lengths (L_e, L_f, T_g) [18] and have allowed laser operation with parameter deviations as large as 10% on the grating period for instance [19]. However, since the optimization process can result in a critical point with less than 1 nm of tolerance [20], a robust design algorithm based on anti-optimization [6] has been combined with the PSOA to provide a HCG mirror which exhibits both a high *MF* and large fabrication tolerances.

2.3 Results

Table 1. Optimum parameters of the HCG obtained by the robust optimization algorithm for a mirror centered at λ_0 = 2.3 µm. Tolerance values which ensure a R_{TM} > 99.5% at λ_0 are presented for each design length.

	Optimum	Tolerances for R_{TM} > 99.5% at λ_0
T_g	713 nm	682 nm < T_g < 773 nm
FF = L_f/Λ	0.484	0.403 < FF < 0.548
T_A	355 nm	255 nm < T_A < 499 nm
Λ	1145 nm	1038 nm < Λ < 1206 nm
T_L	249 nm	215 nm < T_L < 301 nm

The robust optimization algorithm has been used to design a mirror centered at λ_0 = 2.3 µm by adjusting the set of parameters {T_g, FF, T_A, Λ, T_L} with FF = L_f/Λ being the Fill Factor of the grating. For the anti-optimization algorithm, we have fixed a lower bound on each parameter tolerance range, by considering the different capabilities of the involved fabrication steps. A minimum tolerance of the Al_xO_y thickness $\Delta T_A = \pm 50$ nm has been chosen since the wet oxidation process renders the control of the Al_xO_y thickness difficult due to a thickness change of the $Al_{0.98}GaAs$ layer during its oxidation. Even though a 50 nm tolerance requirement is large, it has been shown that HCGs exhibit good tolerances on the thickness of the low index sublayer [21, 15] and is not critical to the algorithm convergence.

The etching of the grating slab is another challenging step of the fabrication process and minimum tolerance values of $\Delta T_g = \pm 20$ nm and $\Delta FF = \pm 0.02$ have been chosen to limit the impact of etching imperfections on the mirror performances. The tolerance requirements of the grating period $\Delta\Lambda$ and the GaAs thickness ΔT_L have been set to 3 nm and 1 nm respectively, since the e-beam nanolithography enables such accuracy.

The robust optimization algorithm returns a design with a large high-reflectivity bandwidth of 369 nm for R_{TM} > 99.5% (Fig. 2) centered at λ_0 = 2.309 µm. The final structure whose dimensions are given in Table 1 fulfills all the tolerance requirements with $\Delta T_A = \pm$ 100 nm, $\Delta T_g = \pm$ 31 nm and $\Delta FF = \pm$ 0.064 (Table 1). The tolerances on the equivalent

#192341 - $15.00 USD Received 18 Jun 2013; revised 8 Aug 2013; accepted 8 Aug 2013; published 3 Sep 2013

parameters (Λ, FF, TA) are quite similar to those presented in ref [19]. The variation ranges given in Table 1 are computed for each parameter independently while keeping the other dimensions at their optimum values. However the fabrication process can result in errors made on several parameters simultaneously. The anti-optimization algorithm can take into account this aspect by varying several dimensions of the structure during the evaluation of the robustness. A statistical study performed on 30 000 tests on the optimum design which parameters are simultaneously and randomly varied within the tolerance requirements shows that 99.9% of the mirrors fulfill the reflectivity requirements with $R_{TM} > 99.5\%$ and $R_{TE} < 90\%$ at $\lambda_0 = 2.3$ μm.

3. Metamorphic growth of VCSEL structure on GaSb

The VCSEL structure is grown by solid-source molecular beam epitaxy (MBE) in a RIBER C21E machine equipped with two valved As and Sb cracker cells providing As_2 and Sb_2. Growth runs were realized on epi-ready Te-doped (100)-oriented GaSb substrates whose temperature was monitored with an optical pyrometer and calibrated using the (1x3) (2x5) reconstruction change. The surface oxide of the substrate was thermally desorbed around 550°C under Sb_2 overflow in order to prevent the Sb desorption from GaSb. The bottom distributed N-doped Bragg mirror (DBR) consists of 24 pairs of Te-doped (10^{18} cm^{-3}) lattice-matched AlAsSb/GaSb, and is grown at 510 °C. The 3λ/4 cavity is grown at 470°C, including $Al_{0.35}Ga_{0.65}As_{0.03}Sb_{0.97}$ cladding layers surrounding five compressively-strained 10 nm-thick $Ga_{0.65}In_{0.35}As_{0.08}Sb_{0.92}$ quantum wells (QWs) separated by 15 nm of AlGaAsSb barriers. Above the cavity, at the first node of electromagnetic field standing wave, a thin GaSb p^{++} (15 nm at $10^{19}cm^{-3}$)/ InAs n^{++}(15 nm at $10^{19}cm^{-3}$) tunnel junction is inserted. The ambipolar role of Si (p-type for Sb-based materials and n-type for As-based materials) is used to dope the TJ in order to limit atoms interdiffusion at the interface.

Above the latter GaSb lattice-matched structure, a metamorphic growth of N-type AlGaAs-based heterostructure is realized, in which two high Al content layers are inserted to achieve by wet thermal oxidation, respectively an oxide confinement aperture, and a fully oxidized low index layer below the HCG. This heterostruture, directly grown on the GaSb/InAs tunnel junction, is composed of GaAs (304 nm)/$Al_{0.98}$GaAs (50 nm)/GaAs (841 nm)/$Al_{0.98}$GaAs (355 nm)/GaAs (713 nm). The lower thin AlGaAs layer is placed at a field node and is devoted to the oxide aperture, while the upper one will serve as the low index layer for insuring a high reflectivity of the HCG. Additionally, thanks to this metamorphic growth of GaAs-based materials, we can benefit from stable etch process for the grating fabrication.

A N-type GaAs layer is then grown directly on the highly doped GaSb/InAs tunnel junction, simply by switching the group III elements. Due to the large lattice mismatch between the InAs and the GaAs (~7%), the strain is relaxed after 1 ML only. After a temporary spotty RHEED pattern, a clear streaky (2x4) pattern, denoting a smooth As-stabilized GaAs surface, is recovered after only 20 ML growth. The position of this metamorphic interface close to the node of the field will ensure minimal optical losses from the generated defects. Indeed, the growth of antimonide material on GaAs [22, 23] or Si [24] substrate and oppositely the growth of GaAs on GaSb have been recently studied [25]. This couple of materials presents the advantage to form defect-free growth capability by confining the propagation of the Lomer misfit dislocations in the plane orthogonal to the growth direction [26]. To study the crystalline quality of the material, high resolution X-ray diffraction (HRXRD) has been carried out using a high resolution Philips X-Pert goniometer. We have used the $Cu_{K\alpha1}$ wavelength from a line focus. The Fig. 2 presents the HRXRD pattern of the VCSEL metamorphic heterostructure on a GaSb (001) substrate, around the (004) reflection. This spectrum evidences a very high crystalline quality and sharp interfaces for the Sb-based materials. In addition, the angular position of the Ga(Al)As-diffraction peaks shows a complete relaxation of these layers.

#192341 - $15.00 USD Received 18 Jun 2013; revised 8 Aug 2013; accepted 8 Aug 2013; published 3 Sep 2013

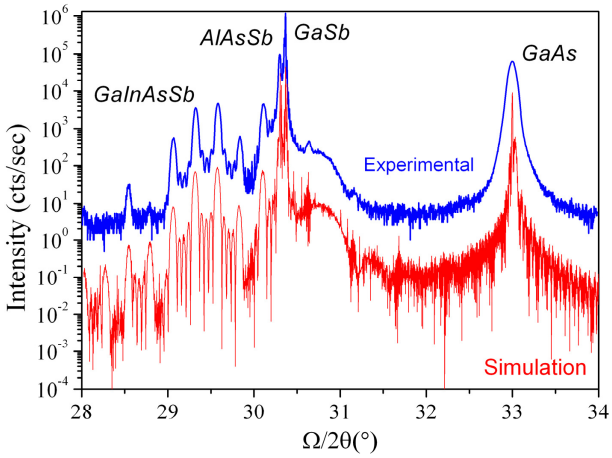

Fig. 2. Experimental and simulated HRXRD patterns of metamorphic half VCSEL grown on GaSb.

The optical reflectivity measured with a Nicolet Fourier transform IR (FTIR) spectrometer shows a stop-band centered at 2.27 µm with a cavity resonance dip at 2.21 µm. This slight detuning can be interpreted by a lower growth rate than estimated during the metamorphic growth of AlGaAs layers. The electroluminescence measurement of this heterostructure was performed just after the growth, on a sample with wide metallic contact pads (500 µm x 500µm) under pulsed operation (1 µs / 21 kHz) at a driving current of 500 mA. The electroluminescence spectrum exhibits a resonantly enhanced emission at 2.21 µm, but the electroluminescence measurement of edge emitted light shows that the QWs gain is centered around 2.32 µm. The reflectivity and electroluminescence spectra measured from the top of the structure are given in Fig. 3.

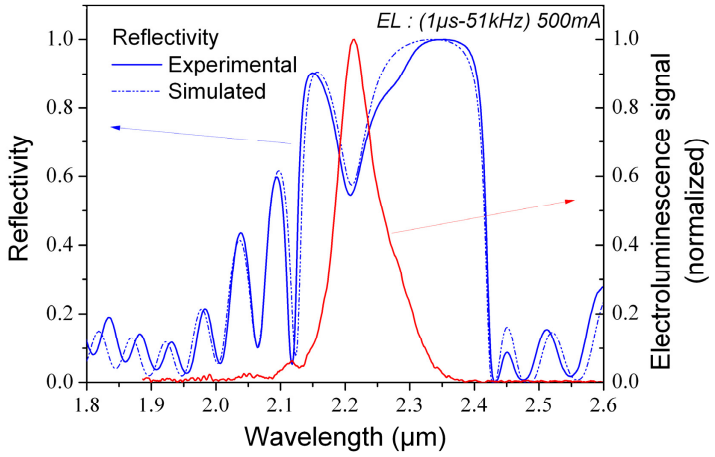

Fig. 3. Reflectivity (experimental and simulation) of the metamorphic half VCSEL after growth and electroluminescence signal of the epitaxial structure.

#192341 - $15.00 USD Received 18 Jun 2013; revised 8 Aug 2013; accepted 8 Aug 2013; published 3 Sep 2013

4. Fabrication of MIR VCSEL structures with HCG mirrors and oxide aperturing

The fabrication process of the HCG-VCSEL is similar to the one of a standard VCSEL. The overall process flow is as follows: the top grating is first realized by nanolithography and inductively coupled plasma reactive ion etching (ICP-RIE), then top ring and substrate backside metallizations are applied, later mesas are formed by ICP-RIE, and afterwards the selective lateral thermal oxidation of both $Al_{0.98}GaAs$ layers simultaneously, is carried out. Subsequently, SiO_2 surface passivation and contact pad deposition are realized. We present now with more insight each of the main fabrication steps for the fabrication of the HCG-VCSEL.

The fabrication of HCG mirror is carried out using the following steps: hard SiO_x mask deposition by plasma-enhanced chemical vapor deposition (PECVD), electron-beam lithography of spin-coated PMMA, ICP-RIE etching of the grating. The etching profile of the grating is critical since it strongly modifies its optical properties. Ideally this profile would be rectangular since the latter geometry presents the highest fabrication tolerance. In any case, the most critical parameter is the grating depth, which fixes the interference conditions between the Bloch modes, and then enables the broadband high reflectivity. In our case, the optimization method described in section 2 gives us a range between 682 and 773 nm for the etch depth, to achieve a sufficient reflectivity with maximum tolerance ranges of the HCG parameters.

To obtain nearly vertical sidewalls, we have developed ICP-RIE etching recipes based on CHF_3 for the hard mask etch, and $Cl_2/N_2/Ar$ for the GaAs layer etch. The Fig. 4 shows the obtained etch profile. The selected GaAs etch was relatively slow, in order to control the groove depth. You may note that the sidewalls have a low roughness thereby minimizing scattering losses.

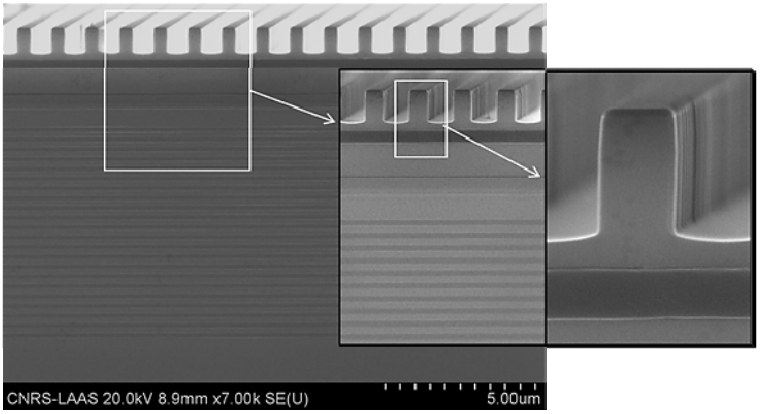

Fig. 4. Cross section image by Scanning Electron Microscopy (SEM) of the fabricated HCG-VCSEL after the ICP-RIE processing.

Hence, a first mesa is etched around the grating down to the N-type GaAs layer below the topmost thick $Al_{0.98}GaAs$ layer, to enable the lateral oxidation of this latter, and the formation of the low-index underneath the HCG. Then a top metal ring contact (TiPtAu) is deposited around the mesa on the N-doped GaAs layer etched surface (Fig. 5). A second larger mesa coaxial with the first one is etched enabling the lateral oxidation of the second $Al_{0.98}GaAs$ layer serving as electrical and optical confinement aperture (see Fig. 6(a)).

This successive realization of these two aligned mesas, will allow to realize the oxidation of the both Al-rich layers in a single run. The goal is to seal completely the oxidation of the upper AlGaAs layer below the HCG, to have a bulk low index layer below the overall surface of the HCG. Since this AlGaAs layer is thicker and that the oxidation proceed from a smaller diameter of mesa, this sealing will occur quite rapidly.

#192341 - $15.00 USD Received 18 Jun 2013; revised 8 Aug 2013; accepted 8 Aug 2013; published 3 Sep 2013

At the same time the second deeper oxide layer forming the confinement aperture should be carefully controlled in order to obtain the aimed final aperture diameter. This may be achieved thanks to the relative low thickness of the layer and the initial large diameter of the mesa from which this second oxidation will proceed.

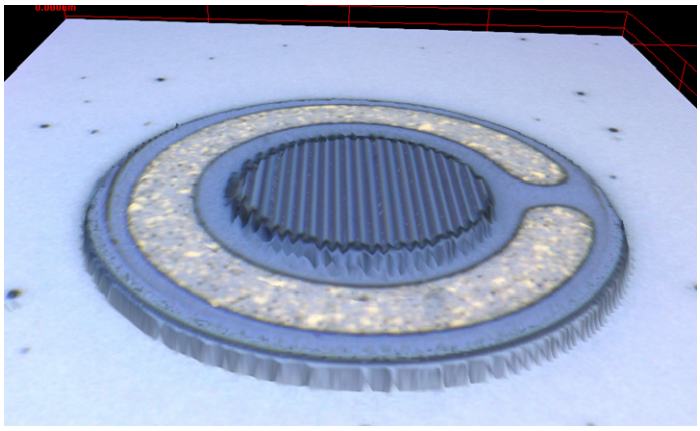

Fig. 5. Confocal microscope image of the processed HCG-VCSEL.

Then, a single oxidation run for both $Al_{0.98}GaAs$ layers is done. The oxidation of the layer below the grating completes first and the process is stopped once the oxide apertures (see Fig. 6(b)) are observed to be slightly smaller than the top grating size (see Fig. 6(a)) . This lateral wet thermal oxidation was performed at 400°C and lasted 102 minutes, and have been monitored in situ by a dedicated infrared imaging setup (see Fig. 6(b)) [27]. At this point, it is interesting to emphasize that the oxidation kinetics and the oxide structural quality of these metamorphic $Al_{0.98}GaAs$ layers is identical to the one obtained with conventional lattice-matched layers on GaAs. Finally, the HCG-VCSEL fabrication is completed by the PECVD deposition of a SiO_x passivation layer, followed by the deposition of the upper contact pad.

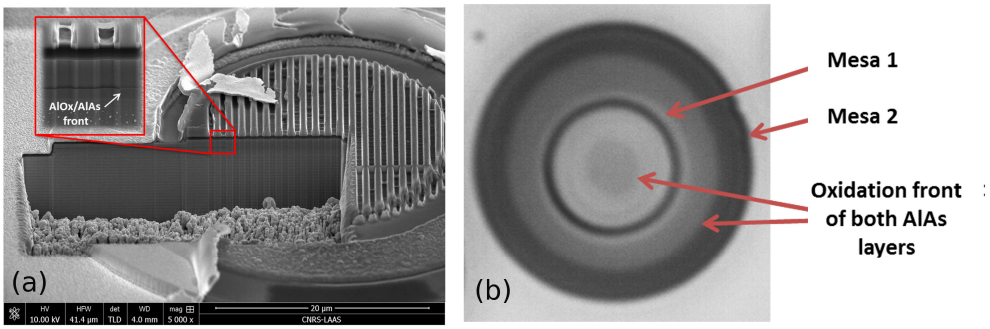

Fig. 6. Images of the HCG-VCSEL during the technological processing. (a) Focused Ion Beam (FIB) image of HCG-VCSEL showing the interface $Al_{0.98}GaAs$ /AlOx of the confinement layer. (b) In situ near-infrared microscope image of the both $Al_{0.98}GaAs$ laterally oxidized layers within the VCSEL structure.

5. Characterizations of the HCG-VCSEL

Optical characterizations under electrical pumping were performed at room temperature and in pulsed mode on the fabricated VCSELs, with gratings size ranging from 19 to 35 µm and oxide apertures ranging from 12 to 28 µm respectively. The voltage-current characteristics show a turn-on voltage of 0.9V to 3V for an applied current around 5mA, with increasing voltage drops from large to smaller apertures. This trend corresponds to the increase of the

#192341 - $15.00 USD Received 18 Jun 2013; revised 8 Aug 2013; accepted 8 Aug 2013; published 3 Sep 2013

series resistance due to current crowding for small aperture sizes. In our designed VCSEL, the goal was not to use small confinement apertures but rather defining an injected carrier profile matching the HCG size. The use of metamorphic AlGaAs layers to realize this lateral confinement has proven its efficiency in several previous works [4, 28, 29]. We have then chosen to define oxide aperture smaller than the HCG mirror to ensure a good overlap between the electromagnetic field profile and the mirror area.

Despite the good electrical characteristics and the good electroluminescence measured just after the epitaxial growth, we couldn't observe laser operation with our devices. On Fig. 7, we present the measure spectrum under pulsed electrical pumping, showing a narrow peak at 2.235 µm due to the resonant cavity effect of the structure. The fact that laser action is not reached is attributed to a lack of reflectivity around 2.25 µm of the HCG mirror, together with a large and unfavorable detuning between the cavity mode and the QW gain centered 2.32 µm. The assumption of low reflective HCG has been confirmed by a cross-section observation with a focus ion beam (FIB) (Fig. 6(a)), revealing substantial deviations of the geometrical parameters of the grating (grating depth, fill factor) from the design. An estimation of the HCG reflectivity with the measured parameters gives a maximum reflectivity around 97.8% at the resonance wavelength, indeed not sufficient to support laser operation.

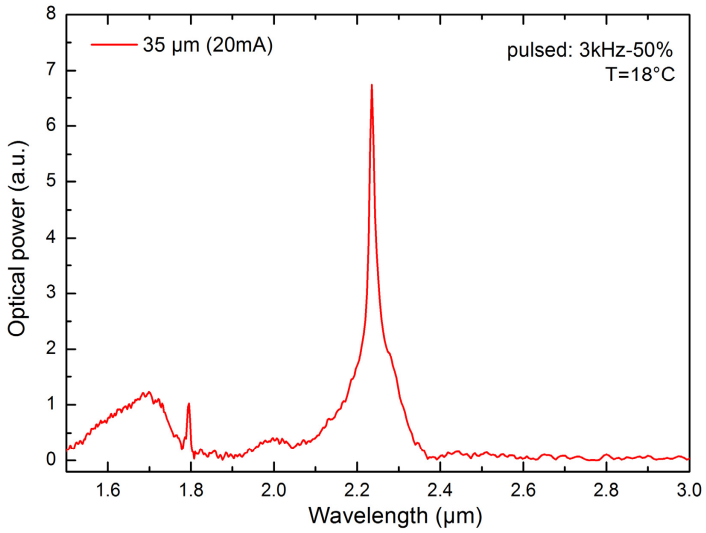

Fig. 7. Electroluminescence spectrum of the MIR HCG-VCSEL in pulsed regime taken at room temperature.

6. Conclusion

In conclusion, we have presented a thorough study on an original GaSb-based VCSEL structure for operation in the MIR range. This MIR VCSEL structure incorporates a lateral oxide confinement and the replacement of the top Bragg mirror by HCG grating mirror. Both elements are formed using the AlGaAs material system metamorphically grown on the GaSb platform, and are expected to significantly improve the performances of the MIR VCSELs and the ability to shape through the design of the grating the output beam properties. We have demonstrated in this work, an original way for designing the VCSEL structure by optimizing the HCG properties while allowing a wide tolerance on geometrical parameters, enabling acceptable margins for the errors during the fabrication process. We have presented the first complete fabrication of such MIR VCSEL structure, including the combination by epitaxial growth of antimonide half-VCSEL structure and metamorphic AlGaAs heterostructures, and the technological process very similar to the standard process flow for near-infrared oxide-

#192341 - $15.00 USD Received 18 Jun 2013; revised 8 Aug 2013; accepted 8 Aug 2013; published 3 Sep 2013

apertured VCSELs. Finally, we show the first demonstration of electrical pumping and light emission at room temperature on this innovative VCSEL structure.

Acknowledgments

This study was supported by the French National Research Agency (ANR), by the program Blanc under the project Marsupilami, Grant NT09-505624. Also, the authors acknowledge the support of RENATECH (the French Network of Major Technology Centres) within the technological platform of LAAS-CNRS.

#192341 - $15.00 USD Received 18 Jun 2013; revised 8 Aug 2013; accepted 8 Aug 2013; published 3 Sep 2013